Tip splitting without interfacial tension and dendritic growth patterns arising from molecular anisotropy

Johann Nittmann* & H. Eugene Stanley†

* Etudes et Fabrication Dowell Schlumberger, 42003 St. Etienne, France
† Center for Polymer Studies and Department of Physics, Boston University, Boston, Massachusetts 02215, USA

Two growth mechanisms of considerable recent interest are related to a single statistical mechanical model. Tip splitting without interfacial tension occurs when a fluid pushes into another miscible fluid of higher viscosity. Dendritic growth occurs when anisotropic molecules aggregate—a common example is the snowflake. We find that both structures are fractal objects, and can be obtained from a single statistical mechanical model, implying that there is a relation between the underlying physical processes involved.

GROWING structures have fascinated mankind for centuries, and today the field of growth phenonena elicits interest from many disciplines, ranging from medicine and biology to fluid mechanics. Two growth forms that have attracted recent interest are the following:

(1) Dendritic growth[1-9]. No two snowflakes are identical; each is assembled by the random aggregation of water molecules. Yet every child can distinguish a snowflake from other growth forms. The key scientific question is by what mechanism the anisotropy of a water molecule becomes amplified from its weak 'local' effect at the molecular level to its pronounced 'global' effect at the macroscopic level of the snowflake.

(2) Tip splitting[10-20]. A classic experiment in fluid mechanics concerns the splitting of a low-viscosity body of fluid which results when it is forced under pressure into a high-viscosity fluid. If the two fluids are immiscible, then the interfacial tension between them serves to establish a length scale at which tip splitting occurs. When the two fluids are miscible there is no interfacial tension, yet tip splitting nonetheless occurs. Thus an important question concerns the physical mechanism which determines the point at which the finger splits.

The scientific questions in (1) and (2) have been the object of research for many years, in part because our present state of understanding is so incomplete[21] that even a little progress would be valuable. The two categories of growth mechanism (1) and (2) have been considered to be quite different, in the sense that the physical basis for one has no relation to that of the other. Here we develop a statistical mechanical model which incorporates both dendritic growth and tip-splitting, thereby relating two disparate fields of enquiry.

Relation between noise and tip splitting

The model is most clearly explained if we begin with the dielectric breakdown model (DBM) of Niemeyer *et al.*[22] on, for example, a triangular lattice. We first place a seed particle at the origin of a large circular domain of radius R. If we think of this seed particle as being the source of a fluid of infinitesimally small viscosity, which is being forced under pressure to displace a fluid with much higher viscosity[23,24], then the interface must move according to Darcy's law:

$$v_n = -\mathbf{n} \cdot \nabla P \tag{1}$$

Here v_n is the velocity component normal to the interface, $\hat{\mathbf{n}}$ is the normal unit vector and P is the pressure field. P is constant in the less viscous fluid and, because $\nabla \cdot \mathbf{v} = 0$, P satisfies the Laplace equation

$$\nabla^2 P = 0 \tag{2}$$

in the more viscous fluid. Hence the relevant boundary conditions are $P(r, \theta) = 1$ anywhere in the low-viscosity body of fluid, and $P(R, \theta) = 0$ along a circle of radius R.

In a perfect medium with radial symmetry and no pressure fluctuations, the interface will spread out in concentric circles. However, because there is always some noise in the system, a fluid-dynamical instability[25] will occur and irregularities in the interface will grow. This noise phenomenon is reproduced in the DBM, which includes fluctuations by means of the following algorithm. First, ∇P is calculated at every perimeter site of the cluster; this is done by solving equation (2) with an overrelaxation technique. At step 1 there is a single seed on a triangular lattice with six perimeter sites. As all sites have equal values of ∇P, the first perimeter site is mapped to the numerical interval $[0, \frac{1}{6}]$ the second to $[\frac{1}{6}, \frac{2}{6}]$, the third to $[\frac{2}{6}, \frac{3}{6}]$ and so forth. Next, a random number generator is used to choose a number in the interval $[0, 1]$. Suppose that this random number is 0.2603238: the second perimeter site is then occupied, and the procedure iterated. For this two-site cluster, ∇P is calculated at the eight perimeter sites, the values are normalized to unity, a new random number is chosen, and one of the eight sites occupied. Such a DBM cluster is characterized by a high degree of noise: as each growth step is determined by only one random number, it is always possible that the random number chosen corresponds to a perimeter site with an extremely small value of ∇P, which by equation (1) should almost never grow. Thus the DBM violates the fundamental Darcy law due to the noise inherent in the algorithm.

We now describe a procedure whereby this noise can be systematically reduced in a controllable fashion. Clearly we need an algorithm such that perimeter sites with extremely small values of ∇P are extremely unlikely to be chosen. This is accomplished by advancing to a new perimeter site only after it has been chosen s times, where s is a parameter which can be tuned. Each perimeter site has a counter which registers how many times that particular site has been chosen. As $s \to \infty$, the growth of the interface will approach Darcy-law growth, in which any point of the interface grows according to the true local pressure gradient. In the Darcy 'zero-fluctuation' or 'mean-field' limit[26] ($s \to \infty$), the interface would be a perfect circle if there were no underlying lattice.

Figure 1*a–c* shows the results of calculations for successive values of s. We find that Fig. 1*b* and *c* resemble tip splitting as observed in the viscous fingering of both newtonian (refs 19, 27; J. D. Chen, personal communication; R. Lenormand, personal communication) and non-newtonian[10,12,18] fluids. When $s = 2$ (Fig. 1*a*), the structure resembles the DBM both qualitatively (although the branches look thicker) and quantitatively

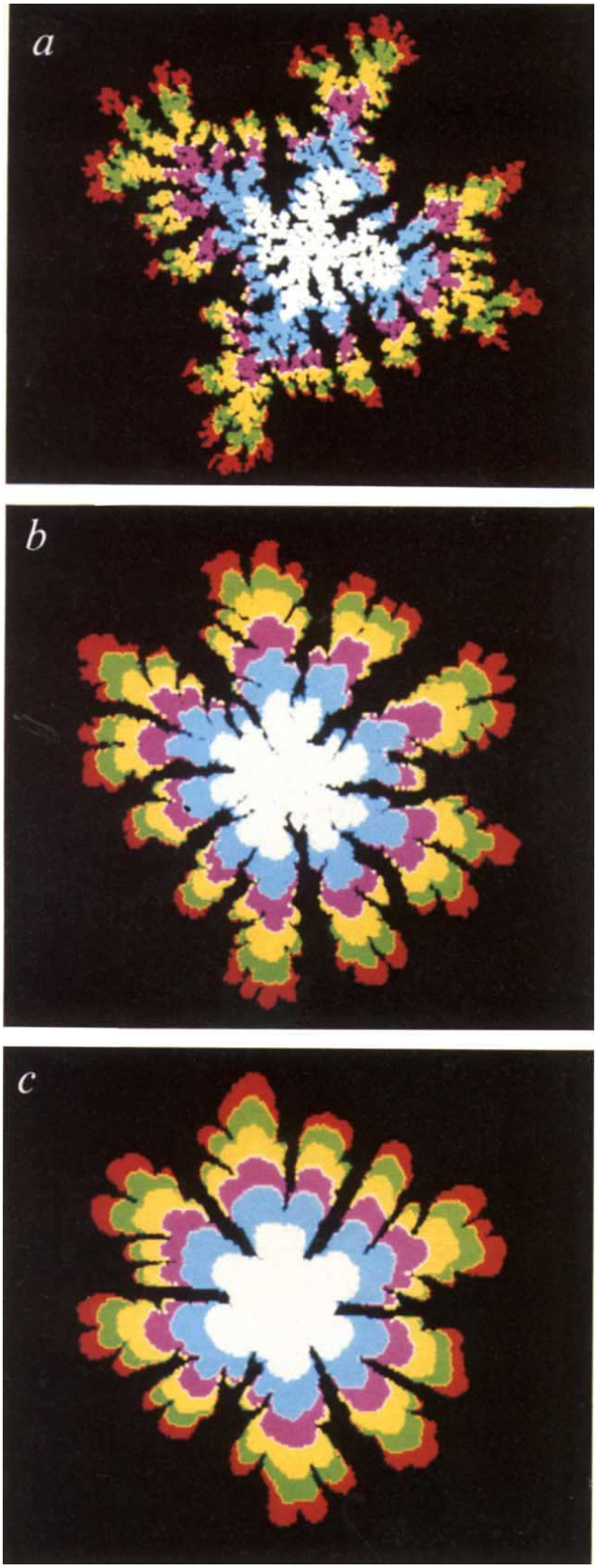

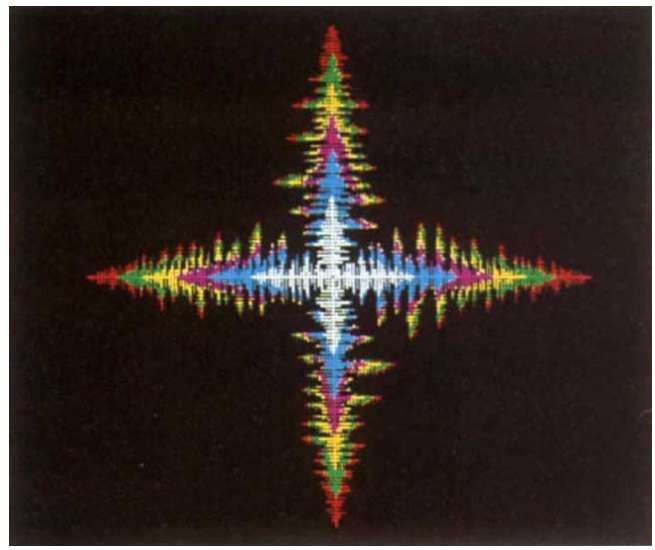

Fig. 2 A typical fractal structure on a square lattice with $s = 50$ and a microscopic anisotropy (defined by equations (6), (7)) of $k - 1 = 10$. The colour coding is the same as in Fig. 1.

($d_f = 1.7$). Here d_f is the fractal dimension obtained, for example, from the slope of a log–log plot of the mass against the caliper diameter. For large s (for example, $s = 20$; Fig. 1*b*), the qualitative appearance appears to differ: the system appears at first sight to cross over to a new 'universality class', with a larger value of d_f. However, when we extrapolate the apparent fractal dimension to large cluster sizes we find that $d_f = 1.7$ for all values of s; that is, the growth forms are quantitatively identical, independent of the degree of noise reduction.

Note that tip splitting always occurs by the same mechanism. First a cluster grows 'smoothly', without tip splitting. However, as the radius of curvature increases, the interface becomes 'rough', with both positive (outward) and negative (inward) fluctuations. The positive fluctuations are not significant, as they are soon damped out; however, the negative fluctuations persist (Fig. 3). This is because, for a charged fractal object, the electric field inside a single notch is very small, and the equation relating the electric field to the gradient of the potential is formally identical to the Darcy law relating growth velocity to the gradient of the pressure. Hence, the tiny notch is not likely to be filled in so quickly as one would expect if interfacial tension were present (Fig. 3*d*). The tiny protrusions on both sides of the notch see a much larger field than does the notch, so they attract mass. The tiny notch thus becomes the terminus of a long fjord (Fig. 3*e*). A fjord is almost perfectly screened, and so is almost never filled in. In Fig. 3, $s = 50$. If $s > 50$ (less noise), then the same tip-splitting mechanism will apply but a negative fluctuation (notch) will decay more efficiently: the system is less susceptible to negative fluctuations and a fjord is formed only when the cluster has reached a larger radius of curvature.

Although the asymptotic fractal dimension d_f is independent of s, the finger thickness W_f clearly increases with s. Moreover, our model explains the existence of a well-defined W_f: the less the noise, the thicker the finger (see Fig. 1). We find the quantitative law:

$$W_f \simeq 4.5 \log s + 2 \qquad (3)$$

Fig. 1 Examples of fractal structures generated when the anisotropy parameter k is held fixed at unity, but the noise parameter $1/s$ is decreased. In *a*, *b* and *c*, $s = 2, 20$ and 200, respectively. For all finite values of s, we find that the fractal dimension is equal to the DBM value, $d_f = 1.7$, providing we take care to extrapolate the apparent mass dependence of d_f to its asymptotic limit. The colour coding is as follows: the first one-sixth of the sites are white, the next sixth are blue, followed by magenta, yellow, green and red.

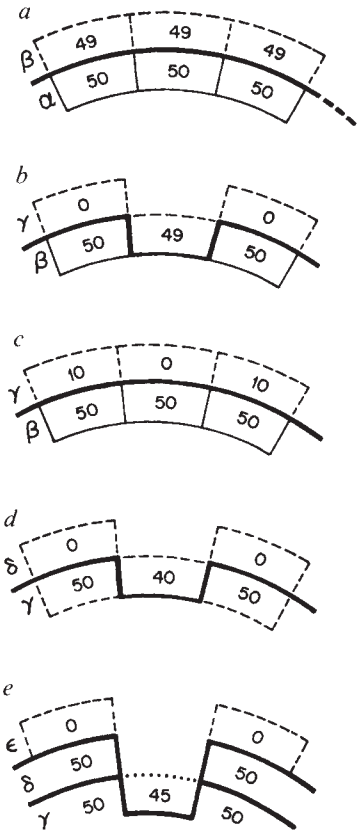

Fig. 3 Schematic illustration of the difference between an outward ('positive') and an inward ('negative') interface fluctuation. A positive fluctuation tends to be damped out rather quickly, as mass quickly attaches to the side of the extra site that is added. On the other hand, a negative fluctuation grows, in the sense that mass accumulates on both sides of the tiny notch. The notch itself has a lower and lower probability of being filled in, as it becomes the end of a longer and longer fjord. This is the underlying mechanism for the tip-splitting phenomenon when no interfacial tension is present. *a* shows the advancing front (row α) of a cluster with $s = 50$. The heavy line separates the cluster sites (all of which were chosen 50 times) from the perimeter sites (all of which have counters registering less than 50). In *a*, no fluctuations in the counters of these three sites have occurred yet, and all three perimeter counters register 49. *b* shows a negative fluctuation, in which the central perimeter site is chosen slightly less frequently than the two on either side; the latter now register 50, and so they become cluster sites in row β. The perimeter site left in the notch between these two new cluster sites grows much less quickly because it is shielded by the two new cluster sites. For the sake of concreteness, let us assume it is chosen 10 times less frequently. Hence by the time the notch site is chosen one more time, the two perimeter sites at the tips have been chosen 10 times (*c*). The interface is once again smooth (row γ), as it was before, except that the counters on the three perimeter sites differ. After 40 new counts per counter, the situation in *d* arises. Now we have a notch whose counter lags behind by 10, instead of by 1 as in *b*. Thus the original fluctuation has been amplified, due to the tremendous shielding of a single notch. Note that no new fluctuations were assumed: the original fluctuation of 1 in the counter number is amplified to 10 solely by electrostatic screening. This amplification of a negative 'notch fluctuation' has the effect that the tiny notch soon becomes the end of a long fjord. To see this, note that *e* shows the same situation after 50 more counts have been added to each of the two tip counters, and hence (by the 10:1 rule) 5 new counts to the notch counter. The tip counters therefore become part of the cluster, but the notch counter has not yet reached 50 and remains a perimeter site. The notch has become an incipient fjord of length 2, and the potential at the end of this fjord is now exceedingly low. Indeed it is quite possible that the counter will never pass from 45 to 50 in the lifetime of the cluster. In our simulations we can see tiny notch fluctuations become the ends of long fjords, and all of the above remarks on the time-dependent dynamics of tip splitting are confirmed quantitatively.

We also find that W_f is independent of the magnitude of the pressure field. To see this, we varied the global pressure gradient by changing the size of our computational grid from 200 to 25 units and found no variation of the finger thickness. This discovery is explained if one considers that the ratio of the local pressure gradient between a site at a finger tip and a site within a fjord does not change if the global pressure gradient is changed: this in turn is a direct consequence of the fact that the pressure field satisfies a Laplace equation.

Previous work on tip-splitting phenomena has focused on explaining the non-zero value of the finger thickness W_f as arising from the presence of interfacial tension σ (ref. 28; see also ref. 29). However this explanation cannot be applied to miscible fluids, such as those used in recent experiments[10,12,18,27,28], because in this case, by definition, $\sigma = 0$. In our model interfacial tension does not exist (that is, σ acts only on the length scale of a single fluid element or 'pixel'); our observed finger thickness is thus related solely to the concept of noise.

Before proceeding further we note that in the limiting case $s = 1$ the DBM is equivalent to diffusion-limited aggregation[30–32] (DLA). The diffusion analogue of the DBM for $s > 1$ is a DLA-type model in which growth occurs only after a perimeter site has been hit by s random walkers. If all the counters are reset to zero after each growth step, then we have the Meakin model[33] or the Kertész–Vicsek model[8], in which growth of the positive fluctuations (the tips) is amplified because a tip of size 1 pixel is more likely to experience the next growth event—so the apparent value of d_f decreases toward unity as the cluster grows. The DLA-type analogue of our DBM-type model in which the counters are not reset to zero after each growth event is the Tang model[26], for which it is not the positive fluctuations (the tips) that display amplified growth but the negative fluctuations (the notches). Amplified growth of negative fluctuations is the characteristic feature of DLA, explaining our result that d_f has its DLA value for all finite values of s.

Thus we conclude that noise reduction—arising from suppression of fluctuations—does not change the overall 'universality class', but does introduce a characteristic finger thickness.

Local anisotropy and dendritic growth

Real growth phenomena are never perfectly isotropic. In fact, anisotropy appears to dominate dendritic crystal growth; thus, for example, a snowflake is recognized by its six-fold anisotropy, although the noise is also reflected in the variability from one snowflake to another[9]. No two are alike, although the eye immediately recognizes the pattern of a snowflake.

The problem of understanding the growth of a snowflake has a rich history. A large class of models has focused on introducing anisotropy in a 'global' or macroscopic fashion by introducing angular variables and assuming that the growth depends sensitively upon these variables[2–4]. Although the resulting patterns have, by virtue of their rules of construction, the requisite six-fold symmetry, their resemblance to real snowflakes is not striking. Moreover, they lack the random variations that seem to characterize real snowflakes and also fractal objects.

A snowflake grows by successive landings of water molecules, and we have therefore focused our attention on how microscopic irregularities in the landing surface can be translated into the macroscopic structure of the snowflake. To reflect the presence of these microscopic irregularities, we must incorporate into our model the essential fact that the landing sites seen by an incoming molecule are not all equivalent. Hence we replace equation (1) by

$$v_n = -\mathbf{n} \cdot (k \nabla P) \tag{4}$$

where the conservation of mass condition $\nabla \cdot \mathbf{v} = 0$ implies that equation (2) is replaced by

$$\nabla \cdot (k \nabla P) = 0 \tag{5}$$

with the same boundary conditions as for $k = 1$. Here the anisotropy parameter $k = k(x, y)$ would be the permeability in a fluid problem.

Consider a square lattice. One simple choice for $k(x, y)$ is (see Fig. 2)

$$k(x, y) = 1 \tag{6}$$

for x or y even,

$$k(x, y) = k > 1 \tag{7}$$

otherwise equations (6) and (7) express mathematically the fact that the surface affinity for incoming water molecules depends on the spatial coordinate: the incoming particles do not see a perfectly smooth and homogeneous 'landing surface'.

Moreover, our anisotropy is fundamentally different from that considered in, for example, refs 4 and 11. Schematically, in these models the interface is moved according to the rule

$$u = f(\kappa) - f(\theta)u_n \tag{8}$$

where u is the growth velocity, $f(\kappa)$ is an interfacial tension term and u_n is essentially the local pressure (or temperature, or concentration) gradient at the interface. The function $f(\theta)$ indicates the extent to which the growth is enhanced along directions separated by an angle θ. In marked contrast, our model assumes that the anisotropy is present on a molecular level at the interface. We assume that along the interface, the affinity for an incoming water molecule alternates from site to site:

$$u = -f(x, y)u_n \tag{9}$$

We believe that our model is more realistic, as an incoming water molecule in snowflake formation cannot possibly sense the angle $\theta = \arctan(y/x)$, but does see a 'landing surface' whose 'attraction' fluctuates from point to point.

Next we consider the effect of tuning the anisotropy parameter k. Figure 5*a–d* shows structures grown with a succession of increasing values of k, ranging from 1.1 to 11. We hold s fixed at the value $s = 50$; if s were too small, then noise effects would complicate visualization of the effect of anisotropy. Figure 5 is for a triangular lattice, for which equations (6) and (7) are replaced by a different rule: we set $k > 1$ for every fifth row of the three principal directions of the lattice (E-W, NE-SW, NW-SE). We see from Fig. 5 that as k increases there is a pronounced change from the isotropic case $k = 1$, and the resulting growth (see, for example, Fig. 5*d*) resembles a 'snowflake' for reasons more subtle than merely the characteristic 6-fold axis of rotation[34]. Using standard methods (for example, all three methods of ref. 18), we measured d_f for this 'snowflake' and found values that decrease with the number of particles used in the calculation. Extrapolating to infinite size, we find[35,36] $d_f = 1.5 \pm 0.1$.

Although the structure at first sight appears to be somewhat ordered, we realize that this is a trick played by the 6-fold axis. In fact, an individual branch is quite disordered, with side branches of all sizes extending from it. The reason $d_f > 1$ is that the side branches occur with many different length scales. This is especially apparent from Fig. 5*d*, where we see from the colour coding that the latest particle to arrive can attach to the side branches as well as to the tip. Figure 5*e* shows real snowflakes with side branches, which show a striking resemblance to the anisotropic simulations of Fig. 5*d*. The differences between Fig. 5*d* and *e* are the subject of current investigation.

We now address the actual structure of the fractal objects in the presence of anisotropy. It is important to note that there are distinct effects that cooperate to generate the final structure obtained. The first effect is the fine structure of the side branches (see Fig. 2), consisting of a set of 'trees' of varying height, as shown schematically in Fig. 4*a*. The trees are mainly without branches, as the anisotropy favours growth only in even-numbered rows or columns of the lattice. However the height of a tree varies widely from one tree to the next, due to the tendency of tall trees to screen shorter trees. An analogous variation in the height of trees has been found by Meakin[37] in his classic studies of DLA on a planar substrate: he found that

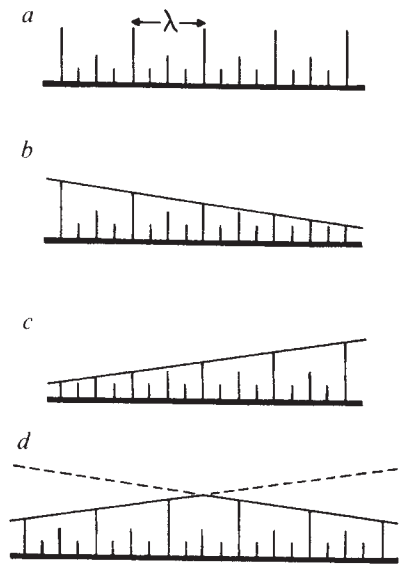

Fig. 4 Schematic illustration to explain the characteristic shape of the four arms of the 'snowflake' cluster in Fig. 2; *a* recalls the fundamental structure of aggregation onto an equipotential surface, first studied by Meakin[37]. For simplicity, the 'trees' are drawn as straight line segments, and the hierachical or fractal distribution of tree height is indicated by a difference of a factor of 2 between successive sizes, together with a spacing, $\lambda(M)$, which increases as M^{1/d_f}, where M is the total cluster mass. *b* shows the modification expected from the fact that the regions of an arm near the centre have more time to accumulate mass than the regions near the tip. *c* shows the effect of the fact that ∇P is much larger near the tip; *d* shows the result of combining *a–c*, and resembles the overall shape observed in Figs 2 and 5*d*.

the resulting fractal structure is a 'forest' of trees, with fewer but taller trees surviving at large times due to their tendency to shield the shorter trees.

The main difference between our work and the Meakin (planar substrate) DLA simulations is our lattice anisotropy (parameterized by $k - 1$) and our noise reduction (parameterized by $1/s$), which have the effect of making the trees tall and straight instead of ramified. Consider now the overall profile for the height of the trees in the side branches. This profile can be understood mathematically as arising from the product of two functions. The first, a decreasing function from origin to tip, is related to the fact that the regions of the branches that were formed at early times tend to be larger than the regions of the branches that were formed at late times (Fig. 4*b*). The second, an increasing function, is related to 'screening'; that is, to ∇P, which is larger near the tips and smaller near the origin (Fig. 4*c*). As $v \propto \nabla P$, the growth rate is larger near the tips. The product of the increasing and decreasing functions gives the characteristic profile for the height of the trees in the side branches (Fig. 4*d*).

We also measured as a function of cluster mass: (1) the caliper width of the side branches of Fig. 2, and (2) the caliper diameter of the entire cluster. Both log-log plots are parallel, with slope $1/d_f$.

Discussion

We have shown that two fundamental physical phenomena that are not yet understood, dendritic growth and tip splitting in the absence of interfacial tension, can be related in that both arise from the same statistical mechanical model—a generalization of the DBM[22]. This means that there are physical features common to both phenomena: they differ only in parameter values. In our model we can incorporate in a direct and systematic fashion the crucial role played by fluctuation phenomena

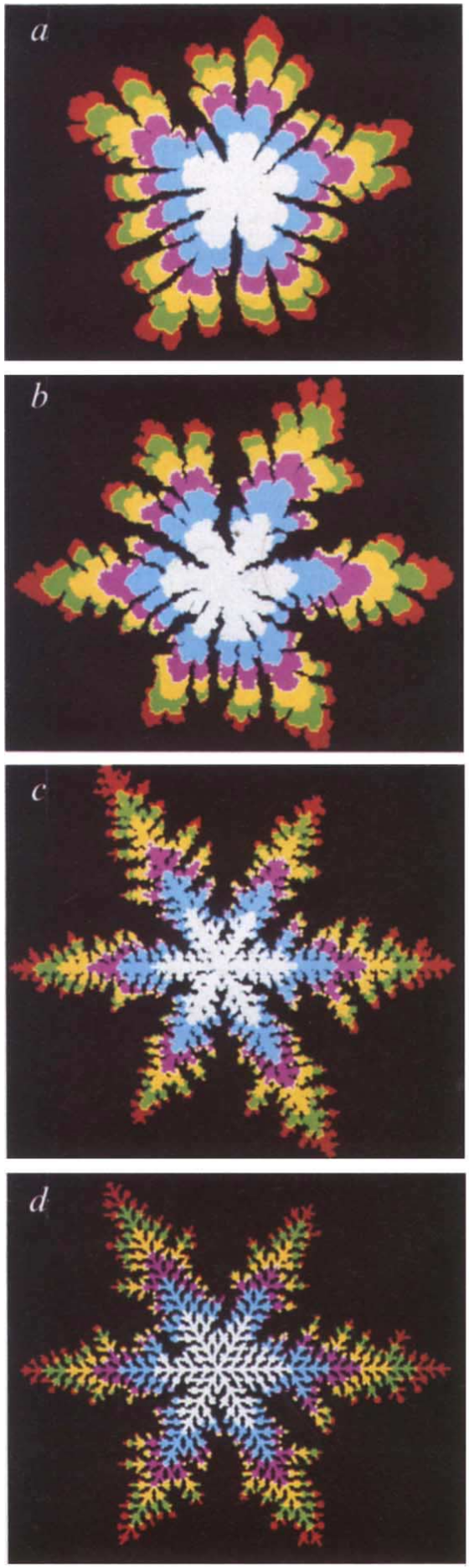

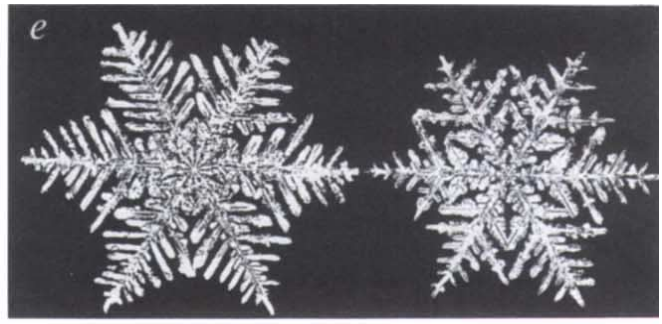

Fig. 5 *a–d*, Examples of fractal structures formed when the noise parameter s is held constant at $s = 50$, but the anisotropy parameter k is chosen to be, respectively, $k-1 = 0.1$, 0.31622, 1.0 and 10.0 (0.31622 interpolates logarithmically between 0.1 and 1.0). The limiting fractal dimension (as mass $\to \infty$) is $d_f \simeq 1.5$, independent of k, for all $k > 1$. The colour coding is the same as in Fig. 1. *e*, Examples of real snowflakes (reproduced with permission from ref. 9) which show a striking resemblance to *d*.

and anisotropy. The physical picture that we have proposed is embodied in two fundamental equations, (4) and (5) (or (1) and (2) for $k = 1$). The second equation describes the spatial change of the pressure field which drives the instability; the first represents the 'growth law', which relates the growth rate of the interface to the pressure field. We have used a generalized Darcy-type law, which enables us to selectively tune both noise and anisotropy.

The overall physical picture that emerges is as follows: Tip-splitting phenomena in the absence of interfacial tension are triggered by microscopic fluctuations (that is, noise). Although positive and negative fluctuations of the interface occur symmetrically, the stability (and hence the subsequent growth) of positive and negative fluctuations are totally different: tip splitting is the direct consequence of this asymmetry in the stability of positive and negative fluctuations. A small protrusion of size 1 pixel is much less long-lived than a small notch of the same size; in fact, it is remarkably difficult to fill even the shallowest notch. Zero noise ($s = \infty$) results in a compact (non-fractal) circular object. A very low noise level (large s) has little effect when a cluster is small, but its effect becomes much more pronounced as the cluster grows larger. In the limit of infinite cluster size, an arbitrarily small but non-zero amount of noise is sufficient to make the cluster fractal. The measured fractal dimension is identical to that of DBM and DLA, two models designed to describe phenomena in the limit in which there is a very high noise level.

The tip-splitting phenomena that occur in the case of zero anisotropy are generalized into a fractal hierachy of side branches in the presence of anisotropy. In the limit of infinite cluster size even a tiny degree of anisotropy changes the fractal dimension from the DLA value of 1.7 to the value 1.5.

Thus, the complete phase diagram has $1/s$ on the abscissa and $(k-1)$ on the ordinate. Asymptotically we find that d_f is constant, at the DBM value of ~ 1.7, everywhere on the x-axis, and d_f is also constant, at the value 1.5, everywhere else in the phase diagram except on the y-axis (zero noise), where $d_f = 1$. Thus noise reduction is not a sufficient perturbation to change d_f from its DBM value, because the negative fluctuations persist for all values of s, and these negative fluctuations control the value of d_f. On the other hand, anisotropy at the microscopic level does change d_f. Further details of this phase diagram suggest an intriguing analogy to critical point phenomena, and this will be the subject of future investigation.

Finally, we return to the question posed in the introduction, of how a tiny anisotropy can become 'amplified' from its local effect at the molecular level to a global effect at the macroscopic

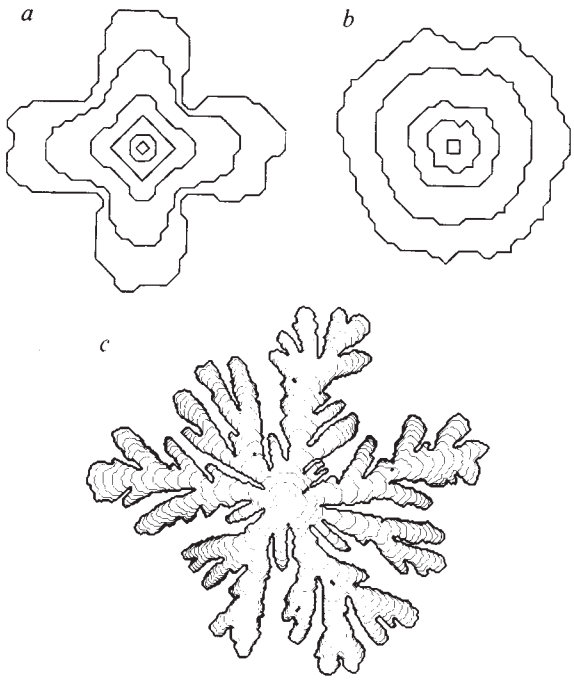

Fig. 6 *a*, Initial growth of an interface on a square lattice for the case $s = 500$. Growth can occur in any of the four space directions (four nearest neighbours). The interface is shown after 5, 21, 85, 200, 500 and 1,000 growth steps. *b*, As in *a*, except that here growth can occur into eight directions (four nearest neighbours and four next-nearest neighbours). The interface is shown after 9, 21, 85, 200, 500 and 1,000 steps. *c*, Viscous fingering structure for $s = 50$, after 15,000 growth steps for eight-fold coordination on a square lattice. The first four contour lines are drawn after 100, 300, 650 and 1,000 steps; subsequent lines are drawn at intervals of 1,000 steps.

level. Our model directly demonstrates this fact: we have shown that in the presence of anisotropy, the resulting fractal dimension is not the DBM value of 1.7, but rather tends asymptotically toward 1.5, a new 'universality class'. Our result is supported by Meakin's very recent calculations for DLA[38] without any local anisotropy, except for that arising from the square-lattice substrate. For this classic and well-studied system, 'pure DLA', Meakin finds the same behaviour that we find in the presence of anisotropy, but only after the cluster size reaches 5 million sites—almost three orders of magnitude larger than the clusters we study! Thus Meakin's local anisotopy, arising solely from the effect of the square lattice itself on the trajectories of random walkers, can lead to a pronounced global effect, altering not only the overall appearance of the cluster but also the fractal dimension itself. As pure DLA is the limit of maximum noise ($s = 1$), we have to wait for an extremely large cluster to see its effect. To support this idea, we systematically reduced s from 50 to 1 while keeping the local anisotropy fixed at the value $k = 2$. When $s = 50$ it is easy to see the snowflake anisotropy pattern, but as s decreases the snowflake vanishes.

To understand better the subtle role played by the anisotropy of the square lattice, we show in Fig. 6*a* the initial growth events for the case $s = 500$, $k = 1$. The early stage of growth is characterized by the competition of 'lattice anisotropy', which attempts to pull the interface into the four principal directions of the plane, and 'interface smoothing' (due to the decay of positive and negative fluctuations), which initially prevents splitting. The competition between these two contradicting tendencies leads to an oscillation of the interface: the structure of the interface alternates between a circle and a diamond-shaped cusp until, eventually, the weak anisotropy of the lattice dominates. As in real systems, no cusp singularities[39] occur: the noise in our systems smooths the sharp corners of the initial cusp as interfacial tension would do. A well-defined finger thickness has developed. The larger the value of s, the smaller is the noise and the larger is W_f. To weaken the lattice anisotropy, which results from the rule that growth is possible only in one of the four space directions (nearest neighbours), we can also allow growth into the four diagonal directions (next-nearest neighbours). Figure 6*b*,*c* shows that such growth is initially almost circular until it reaches a critical radius, after which negative fluctuations are no longer filled in. This gives rise to the characteristic fingering structure shown in Fig. 6*c*. Thus this model seems to represent both qualitatively and quantitatively the viscous fingering phenomenon for the case of miscible fluids (zero interfacial tension).

We thank G. Daccord, R. Lenormand and J. D. Chen for sharing their experimental results with us before publication, and we also thank them and F. Rondelez for helpful discussions. We thank David Kamins for generous and patient assistance with colour computer graphics, and the Boston University Academic Computer Center for generous computer time on the mainframe IBM-3090 computer.

Received 19 December 1985; accepted 21 April 1986.

1. Langer, J. S. *Rev. mod. Phys.* **52,** 1 (1980).
2. Ben-Jacob, E., Goldenfeld, N., Langer, J. S. & Schön, G. *Phys. Rev.* A**29,** 330-340 (1984).
3. Brower, R. C., Kessler, D. A., Koplik, J. & Levine, H. *Phys. Rev.* A**29,** 1335-1342 (1984).
4. Kessler, D. A., Koplik, J. & Levine, H. *Phys. Rev.* A**30,** 2820-2823 (1984).
5. Honjo, H., Ohta, S. & Sawada, Y. *Phys. Rev. Lett.* **55,** 841-844 (1985).
6. Vicsek, T. *Phys. Rev. Lett.* **53,** 2281-2284 (1984).
7. Szép, J., Cserti, J. & Kertész, J. *J. Phys.* A**18,** L413-L416 (1985).
8. Kertész, J. & Vicsek, T. *J. Phys. A* (in the press).
9. Bentley, W. A. & Humphreys, W. J. *Snow Crystals* (Dover, New York, 1962).
10. Nittmann, J., Daccord, G. & Stanley, H. E. *Nature* **314,** 141-144 (1985).
11. Sander, L. M., Ramanlal, P. & Ben-Jacob, E. *Phys. Rev.* A**32,** 3160-3165 (1985).
12. Van Damme, H., Obrecht, F., Levitz, P., Gatineau, L. & Laroche, C. *Nature* **320,** 731-733 (1986).
13. DeGregoria, A. J. & Schwartz, L. W. *J. Fluid Mech.* **164,** 383-400 (1986).
14. Bensimon, D. *Phys. Rev.* A**33,** 1302-1308 (1986).
15. Lenormand, R. & Zarcone, C. *Phys. chem. Hydrodyn.* **6,** 497-506 (1985).
16. Chen, J. D. & Wilkinson, D. *Phys. Rev. Lett.* **55,** 1892-1895 (1985).
17. Måløy, K. J., Feder, J. & Jøssang, T. *Phys. Rev. Lett.* **55,** 2688-2691 (1985).
18. Daccord, G., Nittmann, J. & Stanley, H. E. *Phys. Rev. Lett.* **56,** 336-339 (1986).
19. Ben-Jacob, E. *et al. Phys. Rev. Lett.* **55,** 1315-1318 (1985).
20. Paterson, L. *J. Fluid. Mech.* **113,** 513-529 (1981).
21. Maddox, J. *Nature* **313,** 93 (1985).
22. Niemeyer, L., Pietronero, L. & Wiesmann, H. J. *Phys. Rev. Lett.* **52,** 1033-1036 (1984).
23. Paterson, L. *Phys. Rev. Lett.* **52,** 1621-1624 (1984).
24. Sherwood, J. D. & Nittmann, J. *J. Phys., Paris* **47,** 15-21 (1986).
25. Saffman, P. G. & Taylor, G. I. *Proc. R. Soc.* A**245,** 312-329 (1958).
26. Tang, C. *Phys. Rev.* A**31,** 1977-1979 (1985).
27. Paterson, L. *Physics Fluids* **28,** 26-30 (1985).
28. Chuoke, R. L., Van Meurs, P. & Van der Pol, C. *Trans. Am. Inst. Min. Engrs* **216,** 188-194 (1959).
29. Mullins, W. W. & Sekerka, R. F. *J. appl. Phys.* **34,** 323-329 (1963).
30. Witten, T. A. & Sander, L. M. *Phys. Rev. Lett.* **47,** 1400-1403 (1981).
31. Witten, T. A. & Sander, L. M. *Phys. Rev.* B**27,** 5686-5697 (1983).
32. Meakin, P. in *On Growth and Form: Fractal and Non-Fractal Pattern in Physics* (eds Stanley H. E. & Ostrowsky, N.) (Nijhoff, Dordrecht, 1985).
33. Meakin, P. *Phys. Rev.* (submitted).
34. Mason, B. J. *Scient. Am.* **204,** No. 1, 120-130 (1961).
35. Jullien, R., Kolb, M. & Botet, R. *J. Phys., Paris* **45,** 395-399 (1984).
36. Ball, R. C., Brady, R. M., Rossi, G. & Thompson, B. R. *Phys. Rev. Lett.* **55,** 1406-1409 (1985).
37. Meakin, P. *Phys. Rev.* A**27,** 2616-2623 (1983).
38. Meakin, P. *Pap. presented at int. Conf. Fragmentation, Form and Flow in Fractured Media* Neve Ilan, 6-9 January (1986).
39. Shraiman, B. I. & Bensimon, D. *Phys. Rev.* A**30,** 2840-2844 (1984).